mathematics

MDPI

Article

A Computationally Efficient Distributed Framework for a State Space Adaptive Filter for the Removal of PLI from Cardiac Signals

Inam ur Rehman [1], Hasan Raza [2], Nauman Razzaq [3], Jaroslav Frnda [4,5,*], Tahir Zaidi [1], Waseem Abbasi [6] and Muhammad Shahid Anwar [7,*]

[1] Department of Electrical Engineering, College of Electrical and Mechanical Engineering (CEME), National University of Science and Technology (NUST), Islamabad 44000, Pakistan
[2] Department of Electrical Engineering, Hamdard University, Islamabad 44000, Pakistan
[3] Department of Electrical Engineering, National University of Technology (NUTECH), Islamabad 44000, Pakistan
[4] Department of Quantitative Methods and Economic Informatics, Faculty of Operation and Economics of Transport and Communications, University of Zilina, 01026 Zilina, Slovakia
[5] Department of Telecommunications, Faculty of Electrical Engineering and Computer Science, VSB Technical University of Ostrava, 70800 Ostrava, Czech Republic
[6] Department of Computer Science & IT, Superior University, Sargodha 40100, Pakistan
[7] Department of AI. Software, Gachon University, Seongnam-si 13120, Republic of Korea
* Correspondence: jaroslav.frnda@uniza.sk (J.F.); shahidanwar786@gachon.ac.kr (M.S.A.)

Abstract: The proliferation of cardiac signals, such as high-resolution electrocardiograms (HRECGs), ultra-high-frequency ECGs (UHF–ECGs), and intracardiac electrograms (IEGMs) assist cardiologists in the prognosis of critical cardiac diseases. However, the accuracies of such diagnoses depend on the signal qualities, which are often corrupted by artifacts, such as the power line interference (PLI) and its harmonics. Therefore, state space adaptive filters are applied for the effective removal of PLI and its harmonics. Moreover, the state space adaptive filter does not require any reference signal for the extraction of desired cardiac signals from the observed noisy signal. Nevertheless, the state space adaptive filter inherits high computational complexity; therefore, filtration of the increased number of PLI harmonics bestows an adverse impact on the execution time of the algorithm. In this paper, a parallel distributed framework for the state space least mean square with adoptive memory (PD–SSLMSWAM) is introduced, which runs the computationally expensive SSLMSWAM adaptive filter parallelly. The proposed architecture efficiently removes the PLI along with its harmonics even if the time alignment among the contributing nodes is not the same. Furthermore, the proposed PD-SSLMSWAM scheme provides less computational costs as compared to the sequentially operated SSLMSWAM algorithm. A comparison was drawn among the proposed PD–SSLMSWAM, sequentially operated SSLMSWAM, and state space normalized least mean square (SSNLMS) adaptive filters in terms of qualitative and quantitative performances. The simulation results show that the proposed PD–SSLMSWAM architecture provides almost the same qualitative and quantitative performances as those of the sequentially operated SSLMSWAM algorithm with less computational costs. Moreover, the proposed PD–SSLMSWAM achieves better qualitative and quantitative performances as compared to the SSNLMS adaptive filter.

Keywords: adaptive noise cancellation; cardiac signal processing; PD–SSLMSWAM; power line interference; state space adaptive filter

MSC: 92C55

check for updates

Citation: Rehman, I.u.; Raza, H.; Razzaq, N.; Frnda, J.; Zaidi, T.; Abbasi, W.; Anwar, M.S. A Computationally Efficient Distributed Framework for a State Space Adaptive Filter for the Removal of PLI from Cardiac Signals. *Mathematics* **2023**, *11*, 350. https://doi.org/10.3390/math11020350

Academic Editor: Paolo Crippa

Received: 28 November 2022
Revised: 30 December 2022
Accepted: 30 December 2022
Published: 9 January 2023

1. Introduction

The cardiac signal represents the electrophysiology of atrial and ventricular depolarization and repolarization of the heart. Additionally, the cardiac signal contains information regarding the structure and conduction of the heart's electrical conduction system. Due to rapid growth in biomedical technologies in the past decade, the acquisition of cardiac signals has also evolved. Therefore, instead of recoding the normal electrocardiogram (ECG) of cardiac patients, high-resolution ECGs (HRECGs), and ultra-high-frequency ECGs (UHF–ECGs) are also monitored by cardiologists for the diagnosis of sudden cardiac death (SCD), atrial and ventricular abnormalities, ventricular electrical dyssynchrony (e-DYS), pericarditis, heart rate variability (HRV), etc. [1–3]. The acquisition of HRECG and UHF–ECG signals provides in-depth details about the high-resolution in the time and frequency domains, assisting cardiologists in the prognosis of critical cardiac diseases [1,2]. Likewise, an electrophysiology study (EPS) monitors the real-time localized cardiac activity through an intracardiac electrogram (IEGM), which provides aid to electrophysiologists for the ablation of particular heart muscles in the case of critical cardiac arrhythmia [3]. On account of these advancements, the frequency band of interest of cardiac signals may vary up to 1 kHz as compared to standard ECG frequency bands of [0–80] Hz; likewise, the HRECG signal has a bandwidth of 500 Hz while the UHF–ECG and IEGM signal frequency bands may increase to 1 kHz in the cases of atrial/ventricular abnormalities, heart rate variability (HRV), etc. [4–6].

Due to a wider frequency band span, the HRECG, UHF–ECG, and IEGM cardiac signals are more prone to different types of external noises, e.g., baseline wander (BW), high-frequency noise, and power line interference (PLI). Among these noises, the PLI is the most usual and catastrophic noise. For example, the cables carrying cardiac signals in cardiac activity monitoring laboratories are vulnerable to electromagnetic interference (EMI). Therefore, the PLI noise cannot be completely eluded from the cardiac signal even though the recording device has a high common mode rejection ratio (CMRR). Moreover, the frequency (i.e., 50 Hz or 60 Hz depending on the region) of the PLI's fundamental component and its harmonics superimpose with the cardiac signal spectrum span, overwhelms critical features that may mislead cardiologists for diagnosis of myocardial infarction. Therefore, the removal of the PLI's fundamental component and its harmonics are challenging tasks while preserving the underlying cardiac activity.

In the literature, numerous techniques have been proposed for PLI removal from cardiac signals [7–13]. One of the most conventional approaches for PLI removal from the observed cardiac signal is notch filtering, which may be implemented through finite impulse response (FIR) and infinite impulse response (IIR) filters [7–9]. However, notch filtering using FIR and IIR filters provides longer observational delays, ringing effects, and non-linear phase distortions, respectively [10–13]. Moreover, PLI removal through notch filtering may distort the underlying cardiac activity, which could mislead the results, especially in the case of the aforementioned critical diseases.

Signal decomposition-based techniques for cardiac signal denoising have been reported in the literature, e.g., the Fourier decomposition (FD) method [14–17], empirical mode decomposition (EMD) [18,19], and eigenvalue decomposition (EVD) [20]. The FD method decomposes the cardiac signal into different frequency bands and takes out the complete frequency band to remove the PLI interference [21]. The elimination of the complete band bestows a critical impact on the denoised cardiac signal. Likewise, the EMD and its modified algorithms [22,23] decompose the PLI signal into different intrinsic mode functions (IMFs). Hence, removing the PLI noise means setting these IMFs to zero, which leads to the loss of significant underlying cardiac activities. Similarly, the EVD-based techniques [24] estimate the PLI interference eigenvectors and, thereafter, remove these eigenvectors for PLI elimination from cardiac signals, which also eradicate some critical features of cardiac signals.

To overcome such a problem, adaptive filtration techniques have been introduced to better handle and retain the underlying cardiac activity intact [25,26]. In this context, Widrow et al. introduced the concept of adaptive noise cancellation (ANC) and Glover et al. applied ANC for PLI removal by adaptively tracking PLI sinusoids with known parameters, such as amplitude, phase, and frequency [27,28]. Later on, H.C. So modified the ANC technique for two unknown parameters, the amplitude and phase of the PLI signal, while the frequency of the observed signal is known [29]. Likewise, Satija modified the ANC algorithm for all three unknown parameters [30]. Therefore, the ANC's need for a reference signal, makes the medical devices expensive.

Overcoming the issues related to reference-based signals for adaptive filtering that state space adaptive filters introduce does not require reference signals for the removal of the PLI interference from cardiac signals [31–34]. On the other hand, the state space adaptive filter provides fast convergence and efficiently handles the frequency drifts on behalf of higher computational costs. Moreover, the computational burden is further increased due to PLI and its harmonics that need to be removed from the cardiac signal [32].

In this paper, the scope of [34] is extended by making it useful for the effective removal of PLI plus its harmonics from HRECCG, UHF–ECG, and IEGM signals. In this context, the parallel distributed state space least mean square with adaptive memory (SSLMSWAM) framework is proposed to adaptively track and eliminate the PLI and its harmonics from these cardiac signals. The proposed PD–SSLMSWAM algorithm provides lesser computational costs compared to the sequentially operated SSLMSWAM algorithm. The simulation results show that the proposed architecture provides lesser computational costs and it shows almost the same qualitative and quantitative performances as compared to the sequentially operated SSLMSWAM algorithm. The remainder of the paper is organized as follows. In Section 2, the generalized state space model for PLI and its harmonics is modeled. The concept's sequentially operated SSLMSWAM algorithm and proposed parallel distributed framework PD–SSLMSWAM along with the computational comparison is explained in Section 3. Section 4 describes the computer simulation results and discussions. Finally, the conclusion is outlined in Section 5.

2. State Space Model of PLI

The cardiac signal is corrupted by the PLI signal at the time instant k and can be modeled as

$$y[k] = x_{cl}[k] + I[k] \tag{1}$$

where $y[k]$ is the contaminated signal, $x_{cl}[k]$ is the pure cardiac signal, and $I[k]$ is the PLI signal, which can be defined as

$$I[k] = \sum_{i=1}^{M} a_i sin(2\pi f i \Delta T k + \theta_i) \tag{2}$$

where M shows the total number of harmonics of the PLI signal, a_i is the amplitude of the ith harmonic component, f is the fundamental frequency component, ΔT is the sampling period, and θ_i is the phase of the ith harmonic. The PLI signal for the fundamental frequency at $i = 1$ can be expressed as.

$$I[k] = a_1 sin(\omega k + \theta_1). \tag{3}$$

where $\omega = 2\pi f \Delta T$ is the frequency in the rad/esc. The state space representation of the PLI model of the 1st harmonic given in (3) has two states, which can be written as.

$$\begin{aligned} x_1[k] &= a_1 sin(\omega k + \theta_1) \\ x_2[k] &= a_1 sin(\omega k + \theta_1 + \pi/2) = a_1 cos(\omega k + \theta_1) \end{aligned} \tag{4}$$

With the help of trigonometric identities, the (4) can be rewritten as.

$$\begin{aligned} x_1[k] &= a_1 sin(\omega k) cos(\theta_1) + a_1 cos(\omega k) sin(\theta_1) \\ x_2[k] &= a_1 cos(\omega k) cos(\theta_1) - a_1 sin(\omega k) sin(\theta_1) \end{aligned} \tag{5}$$

By rewriting (5) in the matrix form, we have

$$\begin{bmatrix} x_1[k] \\ x_2[k] \end{bmatrix} = \begin{bmatrix} cos(\omega k) & sin(\omega k) \\ -sin(\omega k) & cos(\omega k) \end{bmatrix} \begin{bmatrix} a_1 sin(\theta_1) \\ a_1 cos(\theta_1) \end{bmatrix} \tag{6}$$

The initial conditions at $k = 0$, (6) can be expressed as

$$\begin{aligned} x_1[0] &= a_1 sin(\theta_1) \\ x_2[0] &= a_1 cos(\theta_1) \end{aligned} \tag{7}$$

Putting the initial conditions as defined in (7) into (6) at $k = 0$, we have

$$\begin{bmatrix} x_1[1] \\ x_2[1] \end{bmatrix} = \begin{bmatrix} cos\omega & sin\omega \\ -sin\omega & cos\omega \end{bmatrix} \begin{bmatrix} x_1[0] \\ x_2[0] \end{bmatrix} \tag{8}$$

Likewise, the generalized form for $k > 1$, (8) can be expressed as

$$\begin{bmatrix} x_1[k+1] \\ x_2[k+1] \end{bmatrix} = \begin{bmatrix} cos\omega & sin\omega \\ -sin\omega & cos\omega \end{bmatrix} \begin{bmatrix} x_1[k] \\ x_2[k] \end{bmatrix} \tag{9}$$

Ideally, the main power lines comprise only fundamental frequency components of 50 Hz or 60 Hz (depending on the regional area). However, in practical situations, the integer multiples of the fundamental frequency component, called harmonics, are also present. Due to the half-wave symmetry property, the power line system only has odd harmonics [35]. Therefore, the generalized PLI state space model for M harmonics can be expressed in (10), which is presented at the top of the next page.

$$\begin{bmatrix} x_1[k+1] \\ x_2[k+1] \\ \vdots \\ x_{2M-1}[k+1] \\ x_{2M}[k+1] \end{bmatrix} = \begin{bmatrix} cos\omega & sin\omega & \cdots & 0 \\ -sin\omega & cos\omega & \cdots & 0 \\ \vdots & \vdots & \ddots & \vdots \\ 0 & \cdots & cosM\omega & sinM\omega \\ 0 & \cdots & -sinM\omega & cosM\omega \end{bmatrix} \begin{bmatrix} x_1[k] \\ x_2[k] \\ \vdots \\ x_{2M-1}[k] \\ x_{2M}[k] \end{bmatrix} \tag{10}$$

3. Methodology

3.1. SSLMSWAM Algorithm

The SSLMSWAM adaptive algorithm is based on the state space model, which provides good tracking capabilities with high accuracy [36]. The unforced discrete time state space model for the removal of PLI plus its harmonics from cardiac signals is defined as.

$$\begin{aligned} \mathbf{x}[k+1] &= \mathbf{A}\mathbf{x}[k] \\ y[k] &= \mathbf{c}\mathbf{x}[k] + v[k] \end{aligned} \tag{11}$$

where $y[k]$ is the observed output signal at time index k, $v[k]$ is the observation noise, $\mathbf{c}$ is the output vector, $\mathbf{x}[k]$ is the state vector, and $\mathbf{A}$ is the state transition matrix. Moreover, for SSLMSWAM adaptive filter modeling, it is assumed that $\mathbf{A}$ and $\mathbf{c}$ should be invertible and full rank, respectively, while their pairs $(\mathbf{A}, \mathbf{c})$ should be l-step observable [37]. Furthermore, the predicted state $\bar{\mathbf{x}}[k]$ that is formulated through the *a priori* estimated state $\hat{\mathbf{x}}[k-1]$ can be written as follows:

$$\bar{\mathbf{x}}[k] = \mathbf{A}\hat{\mathbf{x}}[k-1] \tag{12}$$

Similarly, the predicted output $\bar{y}[k]$ and the prediction error $\epsilon[k]$ can be defined as

$$\bar{y}[k] = \mathbf{c}\bar{\mathbf{x}}[k] \tag{13a}$$
$$\epsilon[k] = y[k] - \bar{y}[k] \tag{13b}$$

The SSLMSWAM is a recursive algorithm that recursively estimates the state $\hat{\mathbf{x}}[k]$ given the prior estimated state $\hat{\mathbf{x}}[k-1]$ on the advent of observation $y[k]$. The SSLMSWAM adaptive algorithm updates the states in a well-known estimator form [38].

$$\hat{\mathbf{x}}[k] = \bar{\mathbf{x}}[k] + \mathbf{k}[k]\epsilon[k] \tag{14}$$

where $\mathbf{k}[k]$ is the observational gain. Likewise, the estimated output $\hat{y}[k]$ and the estimated error $e[k]$ can be defined as

$$\hat{y}[k] = \mathbf{c}\hat{\mathbf{x}}[k] \tag{15a}$$
$$\epsilon[k] = y[k] - \hat{y}[k] \tag{15b}$$

The observational gain for SSLMS can be expressed as [39].

$$\mathbf{k}[k] = \mu\mathbf{G}\mathbf{c}^T \tag{16}$$

where μ is the step size, which controls the convergence rate while the matrix $\mathbf{G}$ is chosen in a way to make the pair $(\mathbf{A} - \mathbf{k}[k]\mathbf{c}\mathbf{A}, \mathbf{k}[k])$ controllable for such an estimator. Likewise, the observational gain for the normalized SSLMS (SSNLMS) can also be represented as [40].

$$\mathbf{k}[k] = \mu\mathbf{G}\mathbf{c}^T(\gamma I + \mathbf{c}\mathbf{c}^T)^{-1} \tag{17}$$

where $\mathbf{c}\mathbf{c}^T$ is the normalization factor and γ is a small number to ensure the invertibility of matrix $\mathbf{c}\mathbf{c}^T$.

The generalized PLI state space model (10) contains the frequency drifts in a real-time scenario; therefore, the state space adaptive filter should adaptively tune the step size to better handle these frequency drifts. Hence, the SSLMS with the adaptive memory iteratively tunes the step-size parameter μ by minimizing the following cost function [37].

$$\mathrm{J}[k] = \frac{1}{2}E\left[\epsilon^T[k]\epsilon[k]\right] \tag{18}$$

where $\epsilon[k]$ is the prediction error defined in (13) and $E[\bullet]$ is the expectation operator. Differentiating $J[k]$ with respect to μ can be written as

$$\nabla_\mu[k] = \frac{\partial J[k]}{\partial\mu} = E\left[\frac{\partial\epsilon^T[k]}{\partial\mu}\epsilon[k]\right] \tag{19}$$

By taking the partial fraction of (13), we have

$$\frac{\partial\epsilon[k]}{\partial\mu} = \frac{\partial}{\partial\mu}\left[y[k] - \mathbf{c}\mathbf{A}\hat{\mathbf{x}}[k-1]\right] = -\mathbf{c}\mathbf{A}\boldsymbol{\Psi}[k-1], \tag{20}$$

where $\boldsymbol{\Psi}[k] = \frac{\partial\hat{\mathbf{x}}[k]}{\partial\mu}$ and $\frac{\partial\epsilon^T[k]}{\partial\mu}$ is a row vector; therefore, (19) can be rewritten as

$$\nabla_\mu[k] = -E\Big[\boldsymbol{\Psi}[k-1]\mathbf{A}^{\mathrm{T}}\mathbf{c}^{\mathrm{T}}\epsilon[k]\Big] \tag{21}$$

Differentiating (14) with respect to μ and using (12), (16) and (20), we have

$$\boldsymbol{\Psi}[k] = \Big(\mathbf{A} - \mathbf{k}[k]\mathbf{c}\mathbf{A}\Big)\boldsymbol{\Psi}[k-1] + \mathbf{G}\mathbf{c}^T\epsilon[k], \tag{22}$$

Moreover, the updated equation of the time-varying step size $\mu[k]$ based on the stochastic gradient method can be defined as [38].

$$\mu[k] = \mu[k-1] - \alpha\nabla_\mu[k], \tag{23}$$

where α is a small positive learning rate parameter. Furthermore, the instantaneous estimate of the scalar gradient $\nabla_\mu[k]$ mentioned in (21) can be taken as

$$\hat{\nabla}_\mu[k] = -\mathbf{\Psi}^T[k-1]\mathbf{A}^{\mathrm{T}}\mathbf{c}^{\mathrm{T}}\epsilon[k], \tag{24}$$

Hence (23) can be rewritten as

$$\mu[k] = \Big[\mu[k-1] - \alpha\mathbf{\Psi}^T[k-1]\mathbf{A}^{\mathrm{T}}\mathbf{c}^{\mathrm{T}}\epsilon[k]\Big]_{\mu_-}^{\mu_+}, \tag{25}$$

where μ_- is the lower limit, which is generally set close to zero and μ_+ is the upper limit that depends on the natural variations in the PLI frequency. The complete SSLMSWAM is summarized in (26), where μ is replaced with $\mu[k]$ in the observational gain (16).

$$\begin{aligned}
\hat{\mathbf{x}}[k] &= \mathbf{A}\hat{\mathbf{x}}[k-1] + \mathbf{k}[k]\epsilon[k] \\
\epsilon[k] &= y[k] - \mathbf{c}\mathbf{A}\hat{\mathbf{x}}[k-1] \\
\mathbf{k}[k] &= \mu\mathbf{G}\mathbf{c}^T \\
\mu[k] &= \Big[\mu[k-1] - \alpha\mathbf{\Psi}^T[k-1]\mathbf{A}^{\mathrm{T}}\mathbf{c}^{\mathrm{T}}\epsilon[k]\Big]_{\mu_-}^{\mu_+} \\
\mathbf{\Psi}[k] &= \Big(\mathbf{A} - \mathbf{k}[k]\mathbf{c}\mathbf{A}\Big)\mathbf{\Psi}[k-1] + \mathbf{G}\mathbf{c}^T\epsilon[k]
\end{aligned} \tag{26}$$

Likewise, the SSNLMS adaptive filter algorithm is summarized in (27)

$$\begin{aligned}
\hat{\mathbf{x}}[k] &= \mathbf{A}\hat{\mathbf{x}}[k-1] + \mathbf{k}[k]\epsilon[k] \\
\epsilon[k] &= y[k] - \mathbf{c}\mathbf{A}\hat{\mathbf{x}}[k-1] \\
\mathbf{k}[k] &= \mu\mathbf{G}\mathbf{c}^T(\gamma I + \mathbf{c}\mathbf{c}^T)^{-1}
\end{aligned} \tag{27}$$

The estimated noise-free cardiac signals $\hat{x}[k]$ can be obtained by taking the difference of the estimated output signal $\hat{y}[k]$ and the contaminated cardiac signal $y[k]$, which can be written as

$$\hat{x}[k] = y[k] - \hat{y}[k] \tag{28}$$

The flow diagram of the sequentially operated SSLMSWAM algorithm is shown in Figure 1.

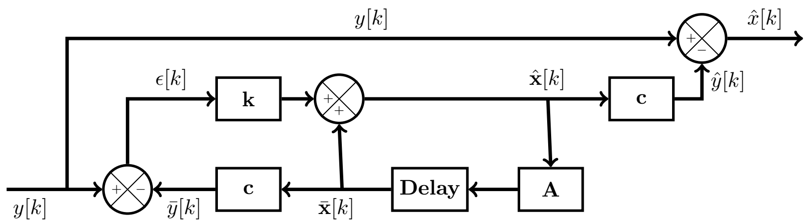

Figure 1. Working of the SSLMSWAM adaptive filter in sequential form.

3.2. Proposed Parallel Distributed System Model

In the conventional SSLMSWAM algorithm, all filter parts are interdependent of each other, which makes the algorithm run in a cascade fashion. Due to the cascade fashion, the SSLMSWAM algorithm provides high computational costs as compared to the SSLMS adaptive filter. However, in the proposed PD–SSLMSWAM algorithm, all filter parts are capable of working in a parallel fashion and this was done by placing the time non-alignment among the parts of the SSLMSWAM algorithm. While setting the time's non-alignment among the participating parts of the algorithm, it must be realized that the behavior of the filter is not uncertain while it implements the desired application; secondly, all of the filter parts are able to operate in a parallel fashion. The flow diagram of the proposed PD–SSLMSWAM is depicted in Figure 2.

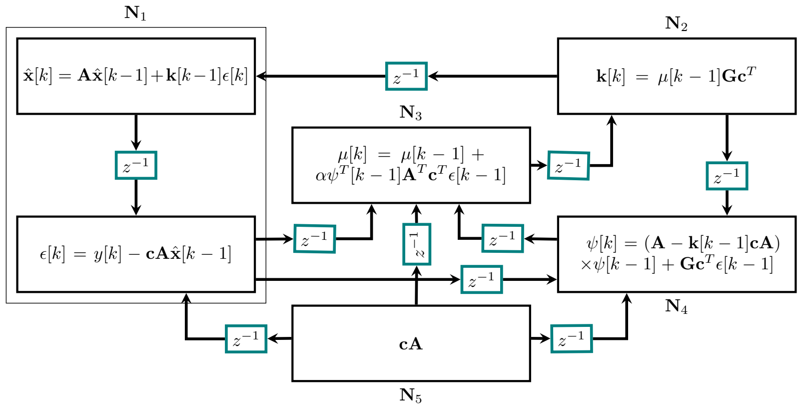

Figure 2. The proposed parallel distributed architecture for the SSLMSWAM adaptive filter.

The sequentially operated state space adaptive filter operated on a single computationally capable unit, as shown in Figure 1. However, if the same state space adaptive filter operates on a group of computationally incapable platforms using the proposed parallel distributed scheme, these filter nodes, namely N_1, N_2, N_3, N_4, and N_5 would be executed parallelly on various individual platforms, as shown in Figure 3.

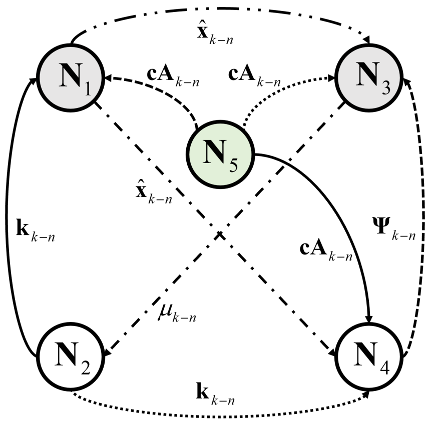

Figure 3. Working procedure for the transmission of data.

Let the processing time taken by the estimated state $\hat{\mathbf{x}}_k$, predicted error ϵ_k, observation gain $\mathbf{k}_k$, step size μ_k, $\mathbf{\Psi}_k$, and $\mathbf{cA}$ be represented as $T_{\hat{\mathbf{x}}}$, T_ϵ, $T_{\mathbf{k}}$, T_μ, $T_{\mathbf{\Psi}}$, and $T_{\mathbf{cA}}$, respectively.

Consequently, the overall time required by the SSLMSWAM algorithm when it operates sequentially can be written as

$$T_{tot} = T_{\hat{\mathbf{x}}} + T_\epsilon + T_{\mathbf{k}} + T_\mu + T_{\mathbf{\Psi}} + T_{\mathbf{cA}} \tag{29}$$

Here, $T_{\mathbf{\Psi}}$ is the maximum contributor to the overall processing time; the strict and sufficient condition based on multiplication and addition computations with respect to fast convergence performance can be defined as

$$T_{\hat{\mathbf{x}}}, T_\epsilon, T_{\mathbf{k}}, T_\mu, T_{\mathbf{cA}} \leq T_{\mathbf{\Psi}} \tag{30}$$

The mismatch factor ξ between the aligned and nonaligned time indexes can be defined as

$$\xi = \|\varepsilon_{seq} - \varepsilon_{NA}\| \tag{31}$$

where ε_{seq} and ε_{NA} are the errors based on the sequentially operated SSRLMSWAM algorithm and proposed PD–SSLMSWAM algorithm, respectively. The pseudocode of the proposed PD-SSLMSWAM is given in Algorithm 1.

Algorithm 1: Pseudocode of the proposed PD-SSLMSWAM

Input: $x_{cl}[k], I[k]$
Output: $\hat{x}[k]$
Initialization: $\alpha \leftarrow 0.0001$
$\mathbf{G} \leftarrow I_{10\times 10}$, $\mu[0] \leftarrow 0.01$
$\hat{x}[0] \leftarrow 0_{10\times 1}$, $\mathbf{k}[0] \leftarrow 0_{10\times 1}$
$\mathbf{c} \leftarrow [1\ 0\ 1\ 0\ 1\ 0\ 1\ 0\ 1\ 0]$
$y[k] \leftarrow x_{cl}[k] + I[k]$
for $k = 1$ *to* n
$\mathbf{A} \leftarrow$ Compute through Equation (10)
Compute $\mathbf{cA}$
Do in Parallel
$\epsilon[k] \leftarrow y[k] - \mathbf{cA}\hat{\mathbf{x}}[k-1]$
$\hat{\mathbf{x}}[k] \leftarrow \mathbf{A}\hat{\mathbf{x}}[k-1] + \mathbf{k}[k-1]\epsilon[k]$
$\mathbf{k}[k] \leftarrow \mu[k-1]\mathbf{G}\mathbf{c}^T$
$\mu[k] \leftarrow \Big[\mu[k-1] - \alpha\Psi^T[k-1]\mathbf{A}^T\mathbf{c}^T\epsilon[k-1]\Big]_{\mu_-}^{\mu_+}$
$\Psi[k] \leftarrow \Big(\mathbf{A} - \mathbf{k}[k-1]\mathbf{cA}\Big)\Psi[k-1] + \mathbf{G}\mathbf{c}^T\epsilon[k-1]$
$\hat{y}[k] \leftarrow \mathbf{c}\hat{\mathbf{x}}[k]$
$\hat{x}[k] \leftarrow y[k] - \hat{y}[k]$

3.3. Computational Complexity

The computational costs of the adaptive algorithm provide significant impacts, particularly in real-time applications. In this section, the complexity comparison of SSNLMS, sequentially operated SSLMSWAM, and proposed PD–SSLMSWAM adaptive filters are discussed. The computational complexity of the sequentially operated SSLMSWAM (26) is given in Table 1 while the computational costs of SSNLMS (27) are mentioned in Table 2. It can be realized that the sequentially operated SSLMSWAM requires $6n^2 + 6n + 1$ multiplications and $6n^2 - n$ additions per iteration. Similarly, the SSNLMS needs $3n^2 + 6n$ multiplications and $3n^2$ additions in each iteration, where n shows the system order.

Table 1. Computational complexity of the SSLMSWAM mentioned in Equation (26).

Eq.#	Operation	Multiplications	Additions
	$\mathbf{d}_{1\times n} = \mathbf{c}_{1\times n}\mathbf{A}_{n\times n}$	n^2	$n^2 - n$
(26.1)	$\hat{\mathbf{x}}[k]_{n\times 1} = \mathbf{A}_{n\times n}\hat{\mathbf{x}}[k-1]_{n\times 1} + \mathbf{k}[k]_{n\times 1}\epsilon[k]_{1\times 1}$	$n^2 + n$	n^2
(26.2)	$\epsilon[k]_{1\times 1} = y[k]_{1\times 1} - \mathbf{d}_{1\times n}\hat{\mathbf{x}}[k-1]_{n\times 1}$	n	n
(26.3)	$\mathbf{k}[k]_{n\times 1} = \mu[k]_{1\times 1}\mathbf{G}_{n\times n}\mathbf{c}^T_{1\times n}$	$n^2 + n$	$n^2 - n$
	$\mathbf{p}_{n\times 1} = \mathbf{d}^T_{n\times 1}\epsilon[k]_{1\times 1}$	n	–
	$\mathbf{q}_{1\times 1} = \mathbf{\Psi}^T[k-1]_{1\times n}\mathbf{p}_{n\times 1}$	n	$n - 1$
(26.4)	$\mu[k]_{1\times 1} = \mu[k-1]_{1\times 1} + \alpha_{1\times 1}\mathbf{q}_{n\times 1}$	1	1
		$2n + 1$	n
	$\mathbf{h}_{n\times 1} = \mathbf{G}_{n\times n}\mathbf{c}^T_{n\times 1}\epsilon[k]_{1\times 1}$	$n^2 + n$	$n^2 - n$
	$\mathbf{J}_{n\times n} = \mathbf{k}[k]_{n\times 1}\mathbf{d}_{1\times n}$	n^2	–
	$\mathbf{O}_{n\times n} = \mathbf{A}_{n\times n} - \mathbf{J}_{n\times n}$	–	n^2
	$\mathbf{s}_{n\times 1} = \mathbf{O}_{n\times n}\mathbf{\Psi}[k-1]_{n\times 1}$	n^2	$n^2 - n$
(26.5)	$\mathbf{\Psi}[k]n \times 1 = \mathbf{s}_{n\times 1} + \mathbf{h}_{n\times 1}$	–	n
		$3n^2 + n$	$3n^2 - n$
	Total	$\mathbf{6n^2 + 6n + 1}$	$\mathbf{6n^2 - n}$

Table 2. Computational complexity of the SSNLMS mentioned in Equation (27).

Eq.#	Operation	Multiplications	Additions
(27.1)	$\hat{\mathbf{x}}[k]_{n\times 1} = \mathbf{A}_{n\times n}\hat{\mathbf{x}}[k-1]_{n\times 1} + \mathbf{k}[k]_{n\times 1}\epsilon[k]_{1\times 1}$	n^2+n	n^2
(27.2)	$\epsilon[k]_{1\times 1} = y[k]_{1\times 1} - \mathbf{c}_{1\times n}\mathbf{A}_{n\times n}\hat{\mathbf{x}}[k-1]_{n\times 1}$	n^2+n	n^2
	$\mathbf{p}_{n\times 1} = \mu_{1\times 1}\mathbf{G}_{n\times n}\mathbf{c}^T_{n\times 1}$	n^2+n	n^2-n
	$q_{1\times 1} = \mathbf{c}_{1\times n}\mathbf{c}^T_{n\times 1}$	n	$n-1$
	$r_{1\times 1} = \gamma_{1\times 1}I_{1\times n} + q_{1\times 1}$	n	1
	$s_{1\times 1} = r^{-1}_{1\times 1}$	1	–
(27.3)	$\mathbf{k}[k]_{n\times 1} = \mathbf{p}_{n\times 1}s_{1\times 1}$	n	–
		n^2+4n+1	n^2
	Total	$\mathbf{3n^2+6n+1}$	$\mathbf{3n^2}$

On the other hand, the proposed PD–SSLMSWAM framework entails less computational costs than sequentially operated SSLMSWAM and SSNLMS adaptive filters. The proposed PD–SSLMSWAM architecture requires parallel $3n^2+n$ multiplications and $3n^2-n$ additions per iteration at maximum, and this reduced complexity is based on the fact that node N_4 provides the maximum computational cost as compared to other nodes in the distributed network, which is clearly presented in Table 1. The summarized forms of complexity comparisons among the proposed PD–SSLMSWAM, sequentially operated SSLMSWAM, and SSNLMS adaptive filters are presented in Table 3. It can be seen that the proposed architecture provides reduced complexity compared to those of sequentially operated SSLMSWAM and SSNLMS adaptive filters.

Table 3. Comparison of computational complexity.

Algorithm	Multiplications	Additions
Sequentially operated SSLMSWAM	$6n^2+6n+1$	$6n^2-n$
SSNLMS	$3n^2+6n+1$	$3n^2$
Proposed PD–SSLMSWAM	$3n^2+n$	$3n^2-n$

3.4. Performance Parameters

Besides the visual inspection, a quantitative measure of the efficiency of the filtering method and the clinical acceptability of the reconstructed signal are employed to provide accurate accessions on the proposed approach. Consequently, four performance evaluation indexes are employed to compare the original (noise-free) cardiac signal with the filtered signal. Therefore, among these performance metrics, the suppression ratio can be written as [41].

$$\gamma = 10log_{10}\left\{\frac{||\mathbf{y}||_2^2}{||\hat{\mathbf{x}}||_2^2}\right\} \tag{32}$$

where $\mathbf{y}$ is the contaminated cardiac signal and $\hat{\mathbf{x}}$ is the filtered signal. in the case of a highly corrupted cardiac signal (low input SNR), the value of the suppression ratio γ should be observed as high as possible.

Secondly, Pearson's correlation coefficient, which shows the shape similarity of the filtered signals to the original noise-free cardiac signals can be expressed as [42]

$$\rho = \frac{E\left[\mathbf{x}\hat{\mathbf{x}}\right]}{\sigma_{\mathbf{x}}\sigma_{\hat{\mathbf{x}}}} \tag{33}$$

where $\sigma_{\mathbf{x}}$ and $\sigma_{\hat{\mathbf{x}}}$ are the standard deviations of pure noise-free cardiac signals and denoised signals, respectively. The value of the correlation coefficient shows the shape similarity of the filtered signals to the original noise-free cardiac signals. Furthermore, the well known SNR and mean square error (MSE) are expressed as [15].

$$SNR_{out} = 10log_{10}\left\{\frac{\sigma^2_{\mathbf{x}}}{\sigma^2_{(\mathbf{x}-\hat{\mathbf{x}})}}\right\} \quad (34)$$

$$MSE = \frac{1}{N}\sum_{n=1}^{N}(x[k] - \hat{x}[k])^2 \quad (35)$$

The output SNR should be high because the remaining interference should be as low as possible. On the other hand, the MSE defines how close the recovered signal is to the clean signal.

4. Results and Discussions

In this section, both the qualitative and quantitative-based results are presented. The proposed PD–SSLMSWAM algorithm is then compared with those of sequentially operated SSLMSWAM and SSNLMS adaptive algorithms. To substantiate the validation of the proposed algorithm, three types of cardiac signals are used in this study, namely, HRECG, UHF–ECG, and IEGM. The HRECG and atrial IEGM signals were acquired from the National Institute of Heart Diseases (NIHD), with a sampling rate of 1000 samples/s and 2000 samples/s, respectively [43]. While the UHF–ECG signal used in this paper is provided by Dr. Pavel Jurak with a sampling rate of 5000 samples/s [4].

4.1. Qualitative Performance

The normalized two-second segment of the pure HRECG signal and its frequency spectrum are shown in Figure 4. The frequency spectrum shows that the recorded HRECG signal has no PLI component or harmonics; however, it contains high-frequency content. The removal of the high-frequency content is not within the scope of this paper, meanwhile the existence of the high-frequency content does not affect the performance of the proposed architecture.

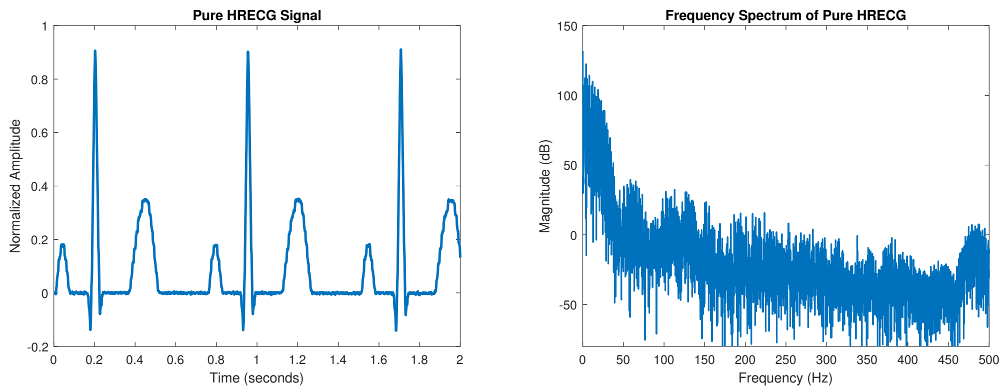

(**a**) (**b**)

Figure 4. Thenoise-free HRECG cardiac signal, plus its frequency spectrum with a sampling rate of 1000 samples/s. (**a**) Pure HRECG signal; (**b**) frequency response of the HRECG test signal.

Moreover, to demonstrate the effectiveness of the proposed algorithm on the significant harmonic content, the following composite PLI interference signal is taken from (2) and can be expressed as

$$\begin{aligned} x_{PLI}(n) = {} & A.1.0sin(\omega n + \theta_1) + A.0.2sin(3\omega n + \theta_3) \\ & A.0.01sin(5\omega n + \theta_5) + A.0.04sin(7\omega n + \theta_7) \\ & A.0.09sin(9\omega n + \theta_9) \end{aligned} \quad (36)$$

where $\omega = 2\pi f_0/f_s$ denotes the normalized angular frequency, $A = 1$ is the amplitude and $\theta_i = \{0°, 180°, 0°, 0°, 180°\}$ are the initial phases of the harmonics of order i. The selected signal is rich in odd harmonic content for being the most usual case for PLI interference. The fundamental frequency of the PLI interference signal is set as f_0 = 48.79 Hz.

To validate the qualitative performance of the proposed algorithm, the PLI noise, with a fundamental frequency of 48.79 Hz, as well as its next four odd harmonics, are considered. The normalized magnitudes of the 1st, 3rd, 5th, 7th, and 9th harmonic components along with the composite PLI signal, are shown in Figure 5. Furthermore, the contaminated HRECG signal with an SNR value of 3 dB is shown in Figure 6. The PLI-contaminated HRECG signal is the mixture of the compound PLI signal and pure HRECG signal. On the other hand, the frequency spectrum of the contaminated HRECG clearly depicts the harmonic as an odd integer multiple of 50 Hz, as illustrated in Figure 6a. For a PLI signal with five harmonic components (including fundamental), the system matrix $\mathbf{A}$ entails the dimensions of 10×10. Likewise, the state vector $\mathbf{w}$ requires the dimension of 10×1 and the observational vector $\mathbf{c}$ entails the dimension of 1×10. For tracking of 1st, 3rd, 5th, 7th, and 9th harmonics of the PLI, the C vector in (15) can be chosen as $\mathbf{c} = [1\,0\,1\,0\,1\,0\,1\,0\,1\,0]$. The SSLMSWAM adaptive filter updates the states based on the recursive approach; therefore, initialization of the parameters, such as α, $\mathbf{G}$, $\hat{\mathbf{x}}[0]$, $\mu[0]$, and $\mathbf{k}[0]$ is required. For the simulation purpose, these parameters are initialized as $\alpha = 0.0001$, $\mathbf{G} = I_{10\times10}$. Moreover, the predicted states $\hat{\mathbf{x}}[k]$ and the observational gain $\mathbf{k}[k]$ are presumed to have zero initial conditions except for $\mu[0]$, which is set to be 0.01. The frequency spectrum of the adaptive tracking of the PLI signal by using the proposed PD–SSLMSWAM architecture is shown in Figure 6b. It can be seen that the proposed architecture provides good tracking for five harmonics components of the PLI signal, including the fundamental component.

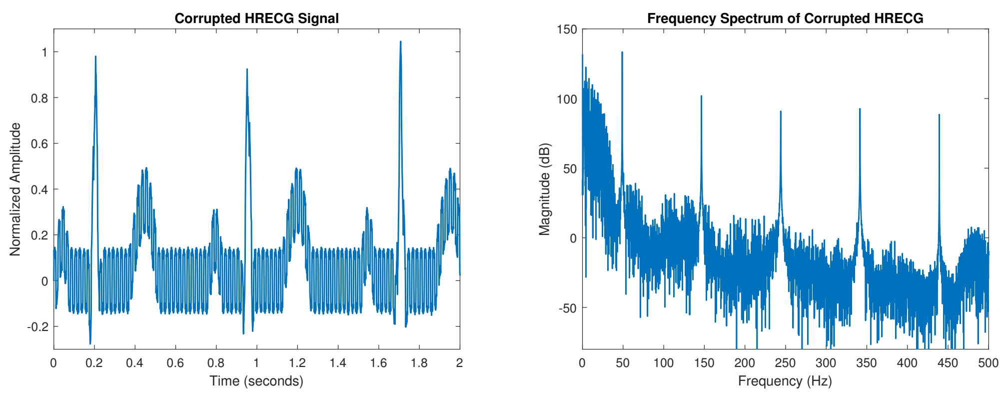

(**a**) (**b**)

Figure 5. The PLI-corrupted cardiac signal plus its frequency spectrum. (**a**) PLI-corrupted HRECG signal; (**b**) the frequency response with the 1st, 3rd, 5th, 7th, and 9th harmonics of PLI.

Furthermore, to validate the qualitative performances of the proposed PD–SSLMSWAM algorithm, a comparison was drawn among the proposed PD–SSLMSWAM adaptive algorithm, sequentially operated SSLMSWAM adaptive algorithm, and the SSNLMS adaptive filter for the PLI interference signal with fundamental and harmonic components. The step size μ is taken as 0.05 for the SSNLMS adaptive filter throughout the rest of the paper. For the simulation, a segment of a PLI-contaminated cardiac signal is shown in Figure 7. The results show that the proposed PD–SSLMSWAM scheme provides an equivalent performance than that of the sequentially operated SSLMSWAM algorithm. However, it is also evident that the transition period of the SSNLMS adaptive filter is greater than that of the proposed PD–SSLMSWAM architecture.

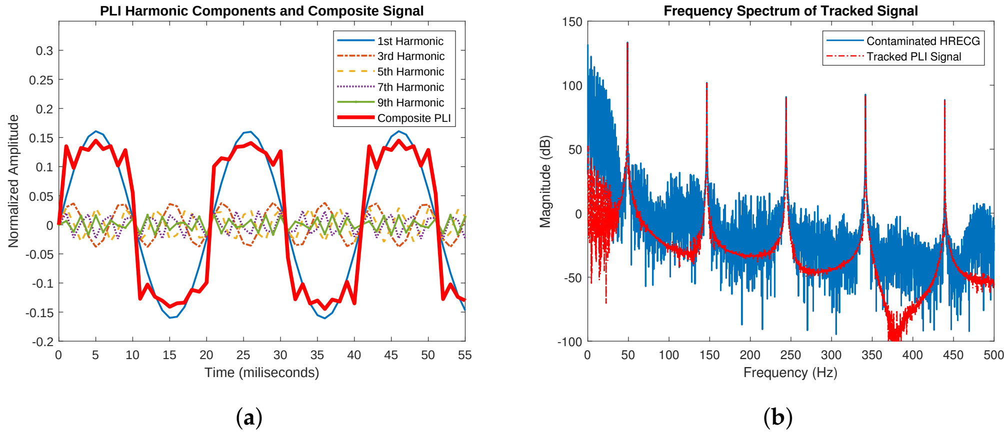

Figure 6. The amplitude scale of PLI harmonics and their tracking. (**a**) The amplitude scale of odd harmonics in the composite PLI signal; (**b**) the frequency spectrum of the tracked PLI signal.

Figure 7. Filtration comparison among the proposed PD–SSLMSWAM, sequentially operated SSLMSWAM, and SSLNLMS adaptive filters for the HRECG cardiac signals.

Likewise, the comparative analysis in terms of the convergence performance for the UHF–ECG signal and IEGM signal are shown in Figures 8 and 9, respectively. It can be observed that the proposed architecture provides almost the same convergence performance as that of the sequentially operated SSLMSWAM algorithm. It can also be realized that the error, which is provided by the proposed PD–SSLMSWAM algorithm, is much less than that of the SSNLMS adaptive filter.

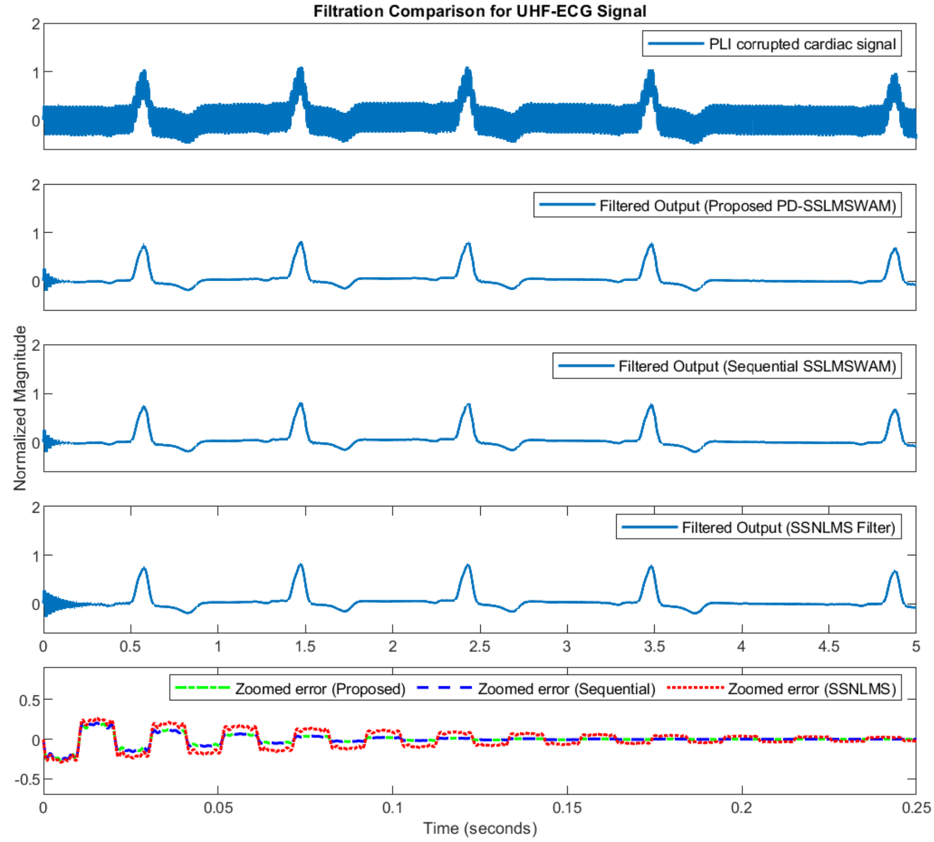

Figure 8. Filtration comparison among proposed PD–SSLMSWAM, sequentially operated SSLMSWAM, and SSLNLMS adaptive filters for the UHF–ECG cardiac signal.

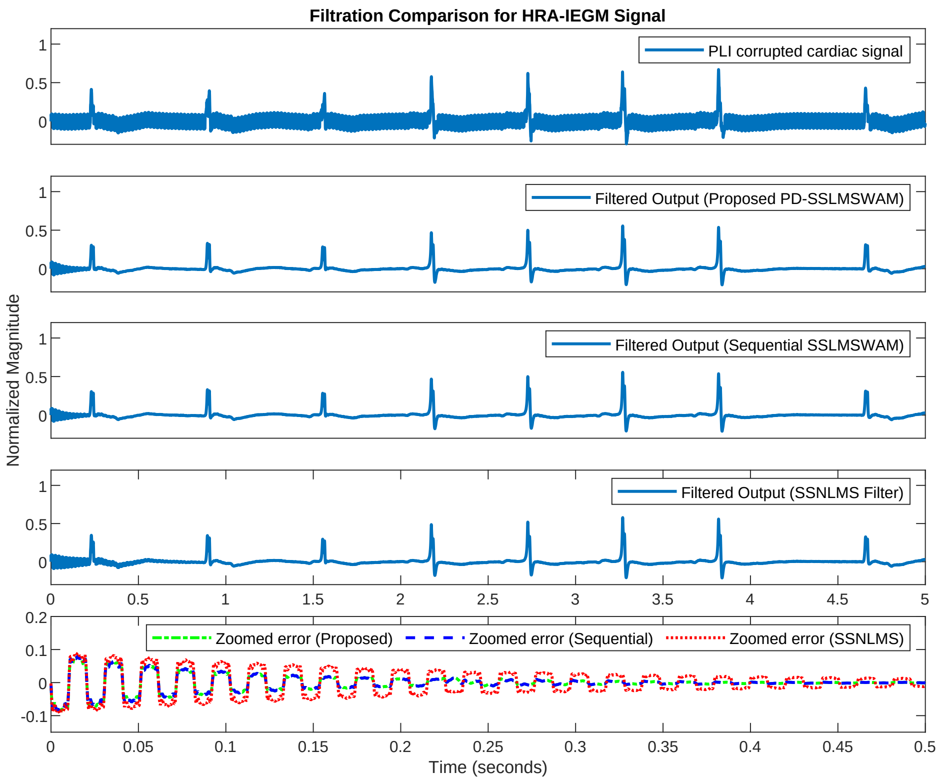

Figure 9. Filtration comparison among the proposed PD–SSLMSWAM, sequentially operated SSLMSWAM, and SSLNLMS adaptive filters for the HRA–IEGM cardiac signal.

The qualitative performance of the proposed PD–SSLMSWAM architecture is almost the same as that of the sequentially–operated SSLMSWAM for all types of cardiac signals. Therefore, the proposed PD–SSLMSWAM algorithm is only compared with the SSNLMS adaptive filter to analyze the convergence performance for abrupt, linear, and sinusoidal deviations in both the amplitude and frequency of the PLI interference. For simulation purposes, a change in the amplitude of the PLI with a range of 0 to 300 mV and a fundamental frequency of 48.79 Hz of the composite PLI signal with a deviation of $\Delta F = \pm 0.75$ Hz are considered.

As the state space adaptive filters track the amplitude of the PLI signal based on the given frequency; therefore, to estimate the change in frequency, the high-resolution frequency estimation technique mentioned in [31] is applied for the proposed PD–SSLMSWAM, sequentially–operated SSLMSWAM, and SSNLMS adaptive filters. Figure 10 shows the corrupted cardiac signal of the PLI with abrupt changes in both the amplitude and frequency of the composite PLI signal. It can be realized that the proposed PD–SSLMSWAM algorithm takes approximately 500 ms, while the SSNLMS adaptive filter requires approximately 1500 ms to track the abrupt deviations in the amplitude and frequency of the PLI signal.

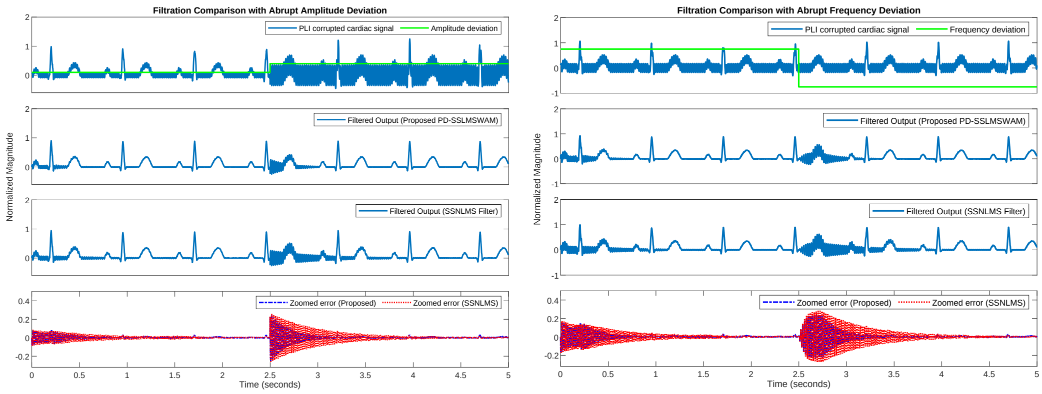

(**a**) (**b**)

Figure 10. Filtration comparison between the proposed PD–SSLMSWAM and SSNLMS adaptive filters for PLI-corrupted cardiac signals.(**a**) Abrupt changes in amplitude; (**b**) abrupt changes in the frequency of the composite PLI signal.

Moreover, the linear deviated PLI-corrupted cardiac signal with respect to amplitude and frequency is shown in Figure 11a and Figure 11b, respectively. It can be observed that the tracking error of the proposed algorithm is less than that of the SSNLMS adaptive filter. Additionally, sinusoidal low variations in the amplitude and frequency of the composite PLI signals are incorporated as shown in Figure 12. It can be evident that the proposed PD–SSLMSWAM algorithm successfully tracks the variations in both the amplitude and frequency of the PLI signal as compared to the SSNLMS adaptive filter.

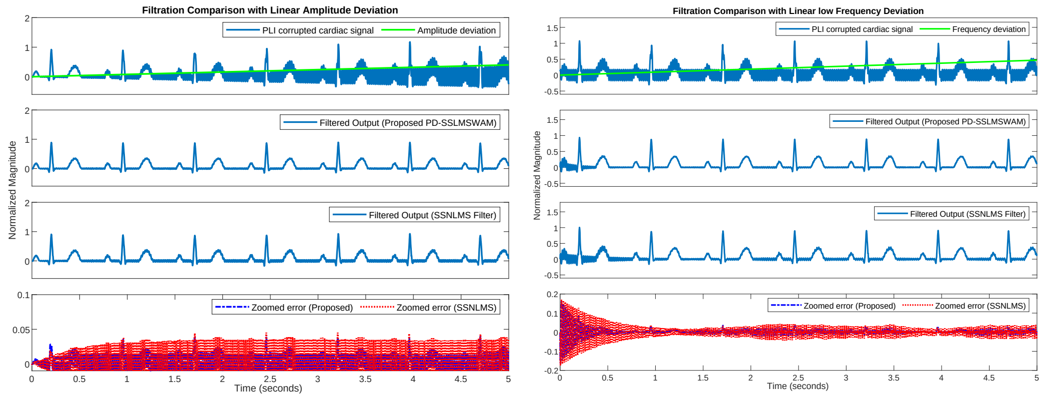

(**a**) (**b**)

Figure 11. Filtration comparison between the proposed PD–SSLMSWAM and SSNLMS adaptive filters for the PLI-corrupted cardiac signals. (**a**) Linear change in the amplitude; (**b**) linear change in the frequency of the composite PLI signal.

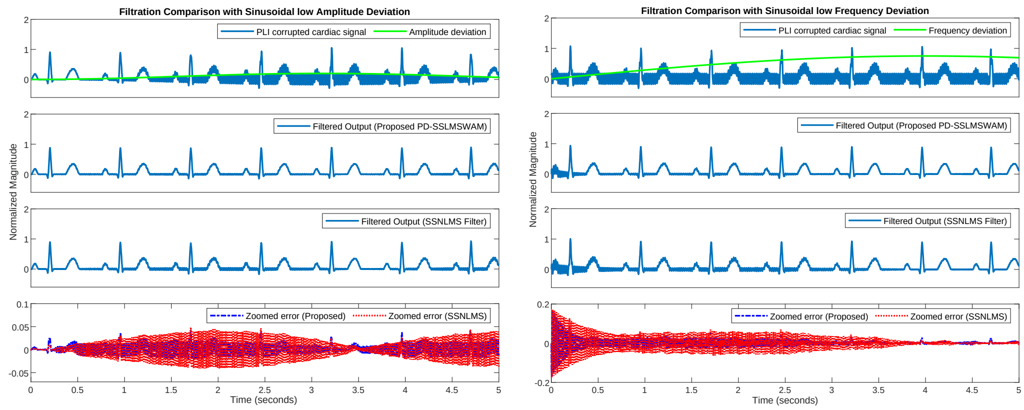

(**a**) (**b**)

Figure 12. Filtration comparison between the proposed PD–SSLMSWAM and SSNLMS adaptive filters for PLI-corrupted cardiac signals.(**a**) Sinusoidal low change in amplitude; (**b**) sinusoidal low change in frequency of the composite PLI signal.

4.2. Qualitative Performance

In this section, the proposed PD–SSLMSWAM technique is compared with those of sequentially operated SSLMSWAM and SSNLMS adaptive filters in terms of computational complexity, suppression ratio [41], correlation coefficient factor [42], the output SNR, and mean square error (MSE) [15].

Figure 13 represents the multiplication and addition complexity comparison of the proposed PD–SSLMSWAM and sequentially operated SSLMSWAM and SSNLMS adaptive filters. It is observed that the proposed technique using nonaligned time indexes parallelly provides lesser multiplication and addition complexities than the sequentially operated SSLMSWAM. However, in the case of the SSLMSWAM adaptive filter, the node N_5 based on $\mathbf{\Psi}[k]$ provides the maximum computational cost as compared to other nodes, as presented in Table 1. Moreover, the parallelly reduced complexity provides serious impacts on the efficiency of the distributed network in terms of less computational costs, which are performed at each processing node.

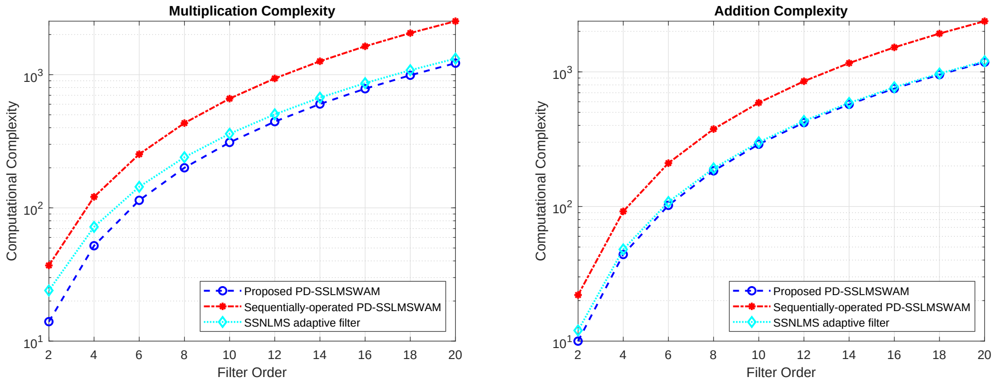

(**a**) (**b**)

Figure 13. Computational complexity comparison among the proposed PD–SSLMSWAM, sequentially operated SSLMSWAM and SSLNLMS adaptive filters. (**a**) Multiplication complexity; (**b**) addition complexity.

The performance criteria of the suppression ratio γ with respect to various SNR values are compared in Figure 14. The proposed PD–SSLMSWAM algorithm has the same suppression ratio as a sequentially operated SSLMSWAM. It is also evident that the SSNLMLS adaptive filter provides much less of a suppression ratio for the low input SNR as compared to the proposed algorithm.

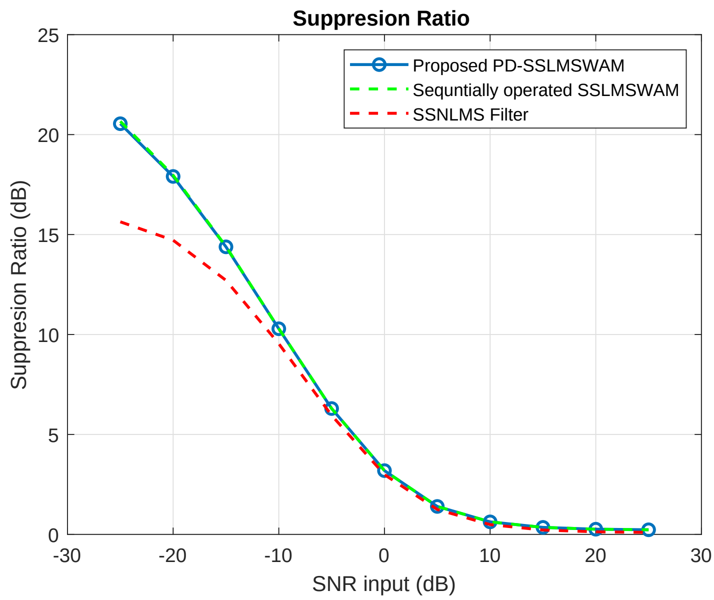

Figure 14. Suppression ratio.

In the cases of critical cardiac diseases, such as SCD, e-DYS, and HRV, the shape or pattern of the cardiac signal helps the cardiologist in the clinical prognosis and diagnosis. Therefore, to measure the shape distortion due to the PLI interference, the correlation coefficient provided by the proposed PD–SSLMSWAM sequentially operates the SSLMSWAM algorithm and the SSNLMLS adaptive filter, as compared in Figure 15. The proposed architecture has almost negligible impacts in terms of shape distortion, while the overall correlation coefficient factor of the SSLMSWAM adaptive filter for the PLI removal is very high even when the corrupted HRECG has an input SNR of -20 dB compared to the SSNLMLS adaptive filter.

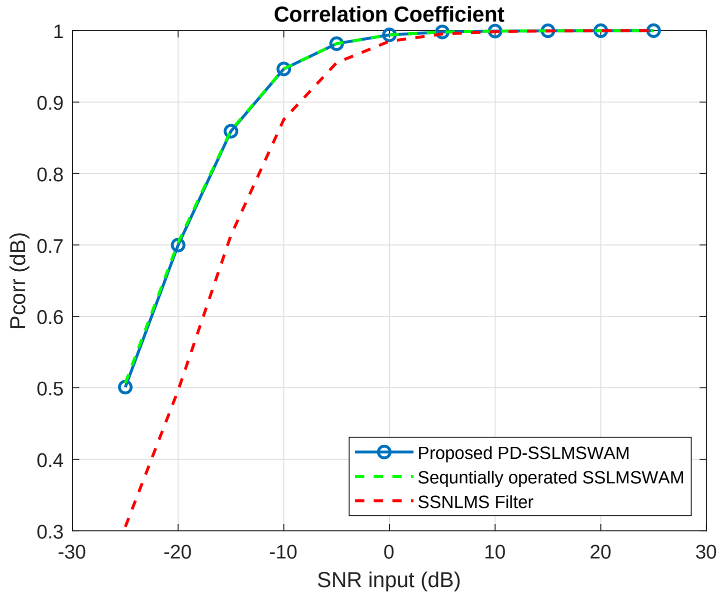

Figure 15. Correlation coefficient.

Furthermore, the comparison between the proposed PD–SSLMSWAM and sequentially operated SSLMSWAM and SSNLMLS adaptive filters for the output SNR and MSE are shown in Figures 16 and 17, respectively. It can be seen that the output SNR provided by the proposed PD–SSLMSWAM architecture is approximately 5 dB higher than that of the SSNLMLS adaptive filter until the input SNR level is 0 dB. Likewise, the MSE error of the proposed architecture is also much less than that of the SSNLMLS adaptive filter.

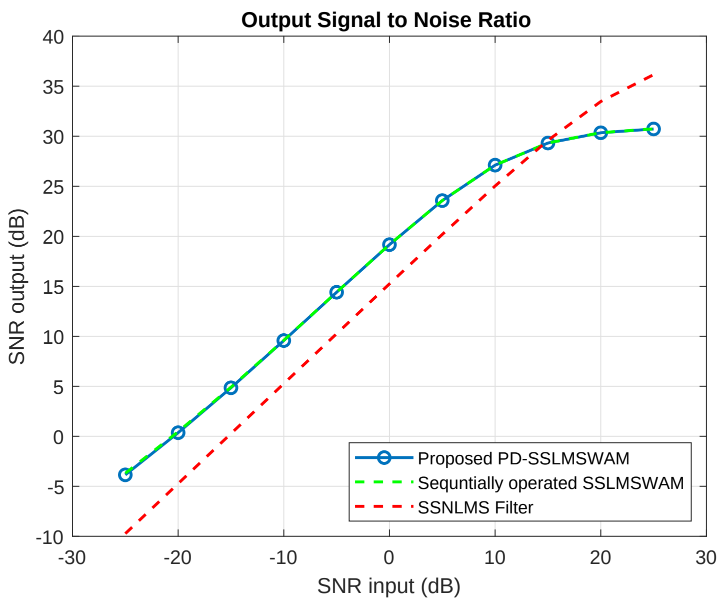

Figure 16. Output signal-to-noise ratio (SNR).

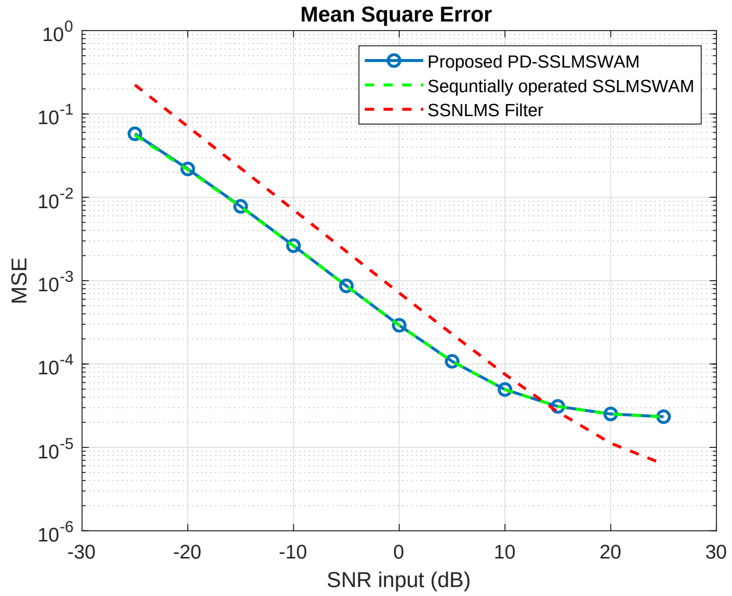

Figure 17. Mean square error (MSE).

Furthermore, to substantiate the validity of the proposed algorithm, a large dataset of real cardiac signals was statistically analyzed to measure the quantitative performance of PD–SSLMSWAM, sequentially operated SSLMSWAM, and SSNLMS adaptive filters. The dataset includes 181 recordings of the HRECG signal, 360 recordings of the UHFECG signal, and 230 recordings of the IEGM signal. Each recording of the real cardiac signal has a length of 30 s. The statistical analysis of the proposed and sequentially operated SSLMSWAM and SSNLMS algorithms for cardiac signals are illustrated in Table 4. The suppression ratios of the proposed and sequentially operated SSLMSWAM are nearly the same for HRECG and IEGM signals, but for the UHFECG signal, the proposed algorithm has more of a suppression ratio than that of the sequentially operated SSLMSWAM. Likewise, the proposed PD-SSLMSWAM algorithm achieves a higher suppression ratio for all three types of cardiac signals compared to the SSNLMS adaptive filter. Moreover, the proposed algorithm provides a much higher output SNR for all three types of cardiac signals, i.e., HRECG, UHFECG, and IEGM than those of the sequentially operated SSLMSWAM and SSNLMS algorithms. Likewise, the correlation coefficients of both the proposed and sequentially operated SSLMSWAM are almost the same for HRECG and IEGM signals, but for the UHFECG signal, the proposed algorithm has a much higher correlation coefficient than that of the sequentially operated SSLMSWAM. Likewise, the proposed PD-SSLMSWAM algorithm achieves a higher suppression ratio for all three types of cardiac signals as compared to the SSNLMS adaptive filter. Furthermore, the proposed algorithm provides a lesser mean square error for all three types of cardiac signals, i.e., HRECG, UHFECG, and IEGM than those of the sequentially operated SSLMSWAM and SSNLMS algorithms.

Table 4. Statistical analysis of the proposed PD–SSLMSWAM, sequentially operated SSLMSWAM, and SSNLMS algorithm for real cardiac data.

Cardiac Data	No. of Recordings	Proposed PD–SSLMSWAM	Sequential SSLMSWAM	SSNLLMS
		Suppression Ratio		
HRECG	181	2.6428	2.3376	2.2778
UHFECG	360	6.8996	0.54561	0.31098
IEGM	230	57.944	57.961	21.566
		Output SNR		
HRECG	181	8342.5	6561.7	6077.6
UHFECG	360	216.25	65.315	27.467
IEGM	230	120.67	118.11	110.62
		Correlation Coefficient		
HRECG	181	0.11652	0.092527	0.086663
UHFECG	360	40.007×10^{-3}	0.303×10^{-3}	0.187×10^{-3}
IEGM	230	0.01332	0.013302	0.079151
		Mean Square Error		
HRECG	181	291.4×10^{-6}	634.85×10^{-3}	25.125
UHFECG	360	4.6085×10^{-6}	205.48×10^{-6}	150.51×10^{-3}
IEGM	230	5.2041×10^{-10}	8.3774×10^{-10}	1.4554×10^{-6}

5. Conclusions

In this paper, a computationally efficient parallel distributed framework for the state space least mean square with an adoptive memory (SSLMSWAM) adaptive filter is proposed. The proposed parallel distributed architecture runs the computationally expensive SSLMSWAM adaptive filter parts in a parallel manner. The proposed parallel distributed SSLMSWAM (PD–SSLMSWAM) algorithm efficiently removes the PLI along with its harmonics (even the time alignments among the contributing nodes are not the same). The proposed PD–SSLMSWAM technique was compared with those of the sequentially operated SSLMSWAM and state space normalized least mean square (SSNLMS) adaptive filters in terms of computational costs and convergence performances. It was observed that the proposed PD–SSLMSWAM algorithm exhibits less computational costs and has nearly the same convergence performance as that of the sequentially operated SSLMSWAM adaptive filter. However, the proposed PD–SSLMSWAM architecture has a high convergence performance for the effective removal of PLI, along with its harmonics from cardiac signals, compared to the SSNLMS adaptive filter.

The source code can be accessed by clicking on the following link.

https://github.com/RaoInam-ur-Rehman/PDSSLMSWAM-for-removal-of-PLI-from-cardiac-signals (accessed on 1 January 2020).

Author Contributions: Conceptualization, N.R., J.F. and W.A.; Methodology, I.u.R. and N.R.; Software, I.u.R., H.R. and T.Z.; Validation, T.Z.; Formal analysis, H.R., N.R., J.F., T.Z., W.A. and M.S.A.; Investigation, W.A.; Resources, M.S.A.; Data curation, H.R., N.R., J.F. and M.S.A.; Writing—original draft, I.u.R.; Writing—review and editing, M.S.A.; Visualization, H.R.; Supervision, T.Z.; Project administration, W.A.; Funding acquisition, J.F. All authors have read and agreed to the published version of the manuscript.

Funding: This research was supported by the Ministry of Education, Youth, and Sports of the Czech Republic under grant SP2023/007 conducted by VSB—Technical University of Ostrava, Czechia, and is partially supported by the institutional research of the Faculty of Operation and Economics of Transport and Communications—University of Zilina, no. 2/KKMHI/2022.

Data Availability Statement: Not applicable.

Conflicts of Interest: The authors declare no conflict of interest.

References

1. De Luna, A.B. *Basic Electrocardiography: Normal and Abnormal ECG Patterns*; John Wiley & Sons: Hoboken, NJ, USA, 2008.
2. Bruce, E.N. *Biomedical Signal Processing and Signal Modeling*; Wiley: New York, NY, USA, 2001.
3. Janson, C.M.; Shah, M.J.; Kennedy, K.F.; Iyer, V.R.; Sweeten, T.L.; Glatz, A.C.; Steven, J.M.; O'Byrne, M.L. Comparison of Outcomes of Pediatric Catheter Ablation by Anesthesia Strategy: A Report from the NCDR® IMPACT Registry. *Circ. Arrhythmia Electrophysiol.* **2021**, *14*, e009849. [CrossRef] [PubMed]
4. Curila, K.; Jurak, P.; Halamek, J.; Prinzen, F.; Waldauf, P.; Karch, J.; Stros, P.; Plesinger, F.; Mizner, J.; Susankova, M.; et al. Ventricular activation pattern assessment during right ventricular pacing: Ultra-high-frequency ECG study. *J. Cardiovasc. Electrophysiol.* **2021**, *32*, 1385–1394. [CrossRef] [PubMed]
5. ur Rehman, I.; Raza, H.; Razzaq, N.; Zaidi, T. Parallel Distributed Framework for State Space Adaptive Filter for Removal of PLI from Cardiac Signals. *Int. J. Bioautomation* **2021**, *25*, 249. [CrossRef]
6. Curila, K.; Jurak, P.; Jastrzebski, M.; Prinzen, F.; Waldauf, P.; Halamek, J.; Vernooy, K.; Smisek, R.; Karch, J.; Plesinger, F.; et al. Left bundle branch pacing compared to left ventricular septal myocardial pacing increases interventricular dyssynchrony but accelerates left ventricular lateral wall depolarization. *Heart Rhythm* **2021**, *18*, 1281–1289. [CrossRef] [PubMed]
7. Piskorowski, J. Powerline interference removal from ECG signal using notch filter with non-zero initial conditions. In Proceedings of the 2012 IEEE International Symposium on Medical Measurements and Applications Proceedings, Budapest, Hungary, 18–19 May 2012; pp. 1–3.
8. Shaik, B.S.; Chakka, V.K.; Goli, S.; Reddy, A.S. Removal of narrowband interference (PLI in ECG signal) using ramanujan periodic transform (RPT). In Proceedings of the 2016 International Conference on Signal Processing and Communication (ICSC), Noida, India, 26–28 December 2016; pp. 233–237.
9. Thomas, C.W.; Huebner, W.P.; Leigh, R.J. A low-pass notch filter for bioelectric signals. *IEEE Trans. Biomed. Eng.* **1988**, *35*, 496–498. [CrossRef] [PubMed]
10. Van Alste, J.A.; Schilder, T. Removal of base-line wander and power-line interference from the ECG by an efficient FIR filter with a reduced number of taps. *IEEE Trans. Biomed. Eng.* **1985**, 1052–1060. [CrossRef]
11. Chavan, M.S.; Agarwala, R.; Uplane, M. Suppression of baseline wander and power line interference in ECG using digital IIR filter. *Int. J. Circuits Syst. Signal Process.* **2008**, *2*, 356–365.
12. Pei, S.C.; Tseng, C.C. Elimination of AC interference in electrocardiogram using IIR notch filter with transient suppression. *IEEE Trans. Biomed. Eng.* **1995**, *42*, 1128–1132.
13. Wang, J.; Ye, Y.; Pan, X.; Gao, X.; Zhuang, C. Fractional zero-phase filtering based on the Riemann–Liouville integral. *Signal Process.* **2014**, *98*, 150–157. [CrossRef]
14. Kumar, A.; Ranganatham, R.; Komaragiri, R.; Kumar, M. Efficient QRS complex detection algorithm based on Fast Fourier Transform. *Biomed. Eng. Lett.* **2019**, *9*, 145–151. [CrossRef]
15. Singh, P. Some Studies on a Generalized Fourier Expansion for Nonlinear and Nonstationary Time Series Analysis. Ph.D. Thesis, IIT Delhi, New Delhi, India, 2016.
16. Shin, H.S.; Lee, C.; Lee, M. Ideal filtering approach on DCT domain for biomedical signals: Index blocked DCT filtering method (IB-DCTFM). *J. Med. Syst.* **2010**, *34*, 741–753. [CrossRef] [PubMed]
17. Bahaz, M.; Benzid, R. Efficient algorithm for baseline wander and powerline noise removal from ECG signals based on discrete Fourier series. *Australas. Phys. Eng. Sci. Med.* **2018**, *41*, 143–160. [CrossRef] [PubMed]
18. Singh, P.; Joshi, S.D.; Patney, R.K.; Saha, K. The Fourier decomposition method for nonlinear and non-stationary time series analysis. *Proc. R. Soc. A Math. Phys. Eng. Sci.* **2017**, *473*, 20160871. [CrossRef] [PubMed]
19. Singh, P.; Srivastava, P.K.; Patney, R.K.; Joshi, S.D.; Saha, K. Nonpolynomial spline based empirical mode decomposition. In Proceedings of the 2013 International Conference on Signal Processing and Communication (ICSC), Noida, India, 12–14 December 2013; pp. 435–440.
20. Jain, P.; Pachori, R.B. An iterative approach for decomposition of multi-component non-stationary signals based on eigenvalue decomposition of the Hankel matrix. *J. Frankl. Inst.* **2015**, *352*, 4017–4044. [CrossRef]
21. Singhal, A.; Singh, P.; Fatimah, B.; Pachori, R.B. An efficient removal of power-line interference and baseline wander from ECG signals by employing Fourier decomposition technique. *Biomed. Signal Process. Control* **2020**, *57*, 101741. [CrossRef]
22. Agrawal, S.; Gupta, A. Fractal and EMD based removal of baseline wander and powerline interference from ECG signals. *Comput. Biol. Med.* **2013**, *43*, 1889–1899. [CrossRef]
23. Rakshit, M.; Das, S. An improved EMD based ECG denoising method using adaptive switching mean filter. In Proceedings of the 2017 4th International Conference on Signal Processing and Integrated Networks (SPIN), Noida, India, 2–3 February 2017; pp. 251–255.
24. Sharma, R.R.; Pachori, R.B. Baseline wander and power line interference removal from ECG signals using eigenvalue decomposition. *Biomed. Signal Process. Control* **2018**, *45*, 33–49. [CrossRef]
25. Guleria, R.; Kaur, R. Removing the power line interference from ECG signal using Kalman least mean square filter. In Proceedings of the 2016 International Conference on Signal Processing, Communication, Power and Embedded System (SCOPES), Paralakhemundi, India, 3–5 October 2016; pp. 1151–1157.

26. Jiao, Y.; Cheung, R.Y.; Mok, M.P. Modified log-lms adaptive filter with low signal distortion for biomedical applications. In Proceedings of the 2012 Annual International Conference of the IEEE Engineering in Medicine and Biology Society, San Diego, CA, USA, 28 August–1 September 2012; pp. 5210–5213.
27. Widrow, B.; Glover, J.R.; McCool, J.M.; Kaunitz, J.; Williams, C.S.; Hearn, R.H.; Zeidler, J.R.; Dong, J.E.; Goodlin, R.C. Adaptive noise cancelling: Principles and applications. *Proc. IEEE* **1975**, *63*, 1692–1716. [CrossRef]
28. Glover, J. Adaptive noise canceling applied to sinusoidal interferences. *IEEE Trans. Acoust. Speech Signal Process.* **1977**, *25*, 484–491. [CrossRef]
29. Martens, S.M.; Mischi, M.; Oei, S.G.; Bergmans, J.W. An improved adaptive power line interference canceller for electrocardiography. *IEEE Trans. Biomed. Eng.* **2006**, *53*, 2220–2231. [CrossRef]
30. Satija, U.; Ramkumar, B.; Manikandan, M.S. Low-complexity detection and classification of ECG noises for automated ECG analysis system. In Proceedings of the 2016 International Conference on Signal Processing and Communications (SPCOM), Bangalore, India, 12–15 June 2016; pp. 1–5.
31. Razzaq, N.; Butt, M.; Salman, M.; Ali, R.; Sadiq, I.; Munawar, K.; Zaidi, T. An intelligent adaptive filter for fast tracking and elimination of power line interference from ECG signal. In Proceedings of the Proceedings of the 26th IEEE International Symposium on Computer-Based Medical Systems, Porto, Portugal, 20–22 June 2013; pp. 251–256.
32. Razzaq, N.; Sheikh, S.A.A.; Salman, M.; Zaidi, T. An intelligent adaptive filter for elimination of power line interference from high resolution electrocardiogram. *IEEE Access* **2016**, *4*, 1676–1688. [CrossRef]
33. Tahir, S.; Raja, M.M.; Razzaq, N.; Mirza, A.; Khan, W.Z.; Kim, S.W.; Zikria, Y.B. Extended Kalman Filter-Based power line interference canceller for electrocardiogram signal. *Big Data* **2021**, *10*, 34–53. [CrossRef]
34. Razzaq, N.; Ullah, E.; Salman, M.; Zaidi, T. State space least mean square adaptive filter for power line interference removal from cardiac signals. In Proceedings of the 2019 IEEE 7th Conference on Systems, Process and Control (ICSPC), Melaka, Malaysia, 13–14 December 2019; pp. 216–221.
35. De La Rosa, F. *Harmonics and Power Systems*; CRC Press: Boca Raton, FL, USA, 2006.
36. Malik, M.B. State-space recursive least-squares: Part I. *Signal Process.* **2004**, *84*, 1709–1718. [CrossRef]
37. Malik, M.B.; Salman, M. State-space least mean square with adaptive memory. In Proceedings of the TENCON 2005-2005 IEEE Region 10 Conference, Melbourne, VIC, Australia, 21–24 November 2005 ; pp. 1–6.
38. Haykin, S.S. *Adaptive Filter Theory*; Pearson Education India: Delhi, India, 2005.
39. Salman, M. Adaptive Estimation Using State-Space Methods. Ph.D. Thesis, National University of Sciences and Technology, Islamabad, Pakistan, 2009.
40. Malik, M.B.; Salman, M. State-space least mean square. *Digit. Signal Process.* **2008**, *18*, 334–345. [CrossRef]
41. Liu, H.; Li, Y.; Zhou, Y.; Jing, X.; Truong, T.K. Joint power line interference suppression and ECG signal recovery in transform domains. *Biomed. Signal Process. Control.* **2018**, *44*, 58–66. [CrossRef]
42. Soedirdjo, S.D.; Ullah, K.; Merletti, R. Power line interference attenuation in multi-channel sEMG signals: Algorithms and analysis. In Proceedings of the 2015 37th Annual International Conference of the IEEE Engineering in Medicine and Biology Society (EMBC), Milan, Italy, 25–29 August 2015; pp. 3823–3826.
43. Armed Forces Institute of Cardiology and National Institute of Heart Diseases. Available online: https://afic.gov.pk (accessed on 27 November 2022).